THE JOURNAL OF PHYSICAL CHEMISTRY A

Article

pubs.acs.org/JPCA

# Lithium Amide ($LiNH_2$) Under Pressure

Dasari L. V. K. Prasad,[†] N. W. Ashcroft,[‡] and Roald Hoffmann*[,†]

[†]Department of Chemistry and Chemical Biology, Cornell University, Ithaca, New York 14853, United States

[‡]Laboratory of Atomic and Solid State Physics, Cornell University, Ithaca, New York 14853, United States

Supporting Information

**ABSTRACT:** Static high pressure lithium amide ($LiNH_2$) crystal structures are predicted using evolutionary structure search methodologies and intuitive approaches. In the process, we explore the relationship of the structure and properties of solid $LiNH_2$ to its molecular monomer and dimer, as well as its valence-isoelectronic crystalline phases of methane, water, and ammonia all under pressure. A $NaNH_2$ (*Fddd*) structure type is found to be competitive for the ground state of $LiNH_2$ above 6 GPa with the $P$ = 1 atm $I\bar{4}$ phase. Three novel phases emerge at 11 ($P\bar{4}2_1m$), 13 ($P4_2/ncm$), and 46 GPa ($P2_12_12_1$), still containing molecular amide anions, which begin to form N−H···N hydrogen bonds. The $P2_12_12_1$ phase remains stable over a wide pressure range. This phase and another $Pmc2_1$ structure found at 280 GPa have infinite ···(H)N···H···N(H)···H polymeric zigzag chains comprising symmetric N···H···N hydrogen bonds with one NH bond kept out of the chain, an interesting general feature found in many of our high pressure (>280 GPa) $LiNH_2$ structures, with analogies in high pressure $H_2O$-ices. All the predicted low enthalpy $LiNH_2$ phases are calculated to be enthalpically stable with respect to their elements but resist metallization with increasing pressure up to several TPa. The possibility of Li sublattice melting in the intermediate pressure range structures is raised.

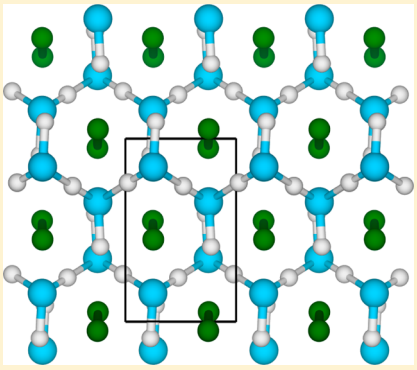

## INTRODUCTION

Condensed lithium amide, $LiNH_2$, is an ionic solid composed of $Li^+$ and $NH_2^-$ (amide) ions, melting at 663 K. Its valence-isoelectronic cousins, $CH_4$, $NH_3$, and $H_2O$, however, exist in molecular gaseous ($CH_4$, $NH_3$) and liquid ($H_2O$) states under standard conditions of $T$ = 298 K, $P$ = 1 atm. In their condensed phases, liquid or solid, the molecules of $CH_4$, $NH_3$, and $H_2O$ are bound either by weak van der Waals interaction or by hydrogen bonds. $LiNH_2$ is very different; clearly, the nature of the inter- and intramolecular forces and the chemical bonding in these compounds (or in fact in any chemical species) plays a crucial role in establishing the physical state of matter at a given $T$ and $P$.

Things change, often drastically so, when one applies external pressure. Methane ($CH_4$)[1,2] and ammonia ($NH_3$)[3,4] crystallize at about 1−2 GPa at 298 K but retain their respective molecular structures, along with orientational disordering. At high pressure and temperatures (19 GPa and 2000−3000 K), methane becomes thermodynamically unstable with respect to heavier hydrocarbons,[5,6] while ammonia transforms (in calculations) into an ionic solid (ammonium amide, $NH_4^+NH_2^-$) at 90 GPa.[7] Water, isoelectronic to the $NH_2^-$ anion, takes a very different path. It loses its well-defined molecular and hydrogen-bonded structure above 60 GPa, forming networks with linear O···H···O symmetrical bridging bonds.[8−10]

What will happen to $LiNH_2$ under pressure? Valence isoelectronic and with analogies to both ammonia and water, whose way will it take? Or will it assume quite different structures? To address these questions, we explore here the high pressure structures of $LiNH_2$ using an evolutionary structure search method and intuitively guided approaches. Our study will show new ground state phases of $LiNH_2$ becoming stable around 6, 11, and 46 GPa, containing orientationally ordered $NH_2$ anions. Structures found at above 11 and 46 GPa have in our calculations N−H···N hydrogen bonding networks quite similar to those in high pressure $NH_3$ (<90 GPa) and $H_2O$-ices (<60 GPa).

At much higher pressures, around 280 GPa, we predict that the ground state of $LiNH_2$ forms infinite zigzag polymer chains with N−H···N hydrogen bonds, approaching symmetrical structures (N···H···N), with one N−H bond not participating in the polymerization. Analogous hydrogen bond symmetrization is observed at lower pressures in ice-X (>60 GPa)[8,9] and phase IV of hydrogen halides, HCl (~51 GPa)[11] and HBr (~39 GPa).[12] Such hydrogen bond symmetrization has so far not been observed in $NH_3$ under pressure but was suggested to present in an as yet unknown phase VI of ammonia (above 55 GPa).[4,13] Interestingly, among the high pressure ionic $NH_3$ structures predicted by Pickard and Needs,[7] the $P2_1/m$ phase that is stable between 331 to 440 GPa contains some symmetric hydrogen bonds between amide ions. The hydrogen bonding pattern we predict is, however, different from those found in ice. Still, we find that, in terms of structure and electrical properties, $LiNH_2$ under pressure may behaves much like $NH_3$ and $H_2O$-ices, respectively.

**Received:** August 7, 2012
**Revised:** September 6, 2012
**Published:** September 14, 2012





dx.doi.org/10.1021/jp3078387 | *J. Phys. Chem. A* 2012, 116, 10027−10036

## RESULTS AND DISCUSSION

**$LiNH_2$ Molecular Structures.** While our main interest here is in solid $LiNH_2$ under compression, it is worthwhile to make a connection to molecular fragments of the solid. Monomeric $LiNH_2$ has been synthesized in the gas phase and its structure was determined by using microwave spectroscopy;[14] its experimental planar geometry is given in Figure 1. Oligomers

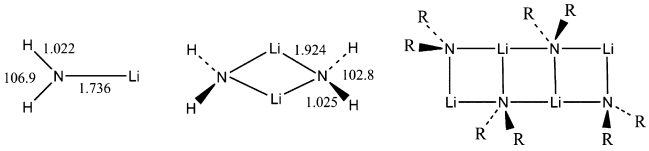


**Figure 1.** Experimental structure of $LiNH_2$ monomer (left), computationally optimized dimer (middle), and a schematic structure of a ladder-like tetramer (right). The bond distances and angles are given in Å and degrees, respectively.

of $LiNH_2$ are organic reagents; as with much lithium chemistry, these molecules, which would readily polymerize to the extended structure if uncoordinated, are stabilized by coordinating bases.[15,16] Few crystal structures of $LiNH_2$ oligomers are known, but we nevertheless have good experimental information from kinetic and nuclear magnetic resonance studies by D. Collum and co-workers and others.[15] In addition to the diborane-like dimer (Figure 1, the structure given is a calculated one), one has evidence for ladder-like oligomers of the type shown in Figure 1, right. Oligomeric cyclic structures are known for substituted lithium amides, $LiNR_2$ ($R$ = an organic group); one sees a range of pretty ring, ladder, cubane structures in this chemistry.[15−17]

The isolated monomer has, as expected, a shorter Li−N separation (1.74 Å) than that found in the ionic solid (2.02 Å). This is the result of Li−N $\pi$-bonding, which is also responsible for the planar configuration at the N. The $LiNH_2$ monomer is not stable against dimerization or oligomerization. The activation-less dimerization energy is calculated to be −2.62 eV; another 0.8 eV is gained in moving to the extended solid. Table 1 also shows the trimerization energy to make clear the energetic path downhill to the crystal. Similar stabilization trends were previously found in our group on studying the links between monomer, dimer, and extended solids of group 2 and 12 dihalides,[18] (in their ground states).

**Table 1. Calculated Nearest Neighbor Bond Distances (Å), H−N−H Angle in $NH_2^-$ (deg), and Association Energies (A.E.) Per Formula Unit (eV/f.u.) of $LiNH_2$ Monomer, Dimer, Trimer, and $I\bar{4}$ Crystal[a]**

| $LiNH_2$ | N−H | Li−N | Li−Li | H−N−H | A.E.* |
|---|---|---|---|---|---|
| monomer [exp][14] | 1.022 | 1.736 | | 106.9 | |
| monomer | 1.022 | 1.740 | | 103.9 | 0.00 |
| dimer | 1.025 | 1.924 | 2.230 | 102.8 | −1.31 |
| trimer | 1.026 | 1.921 | 2.876 | 102.8 | −1.58 |
| crystal ($I$-4) | 1.028 | 2.047 | 2.503 | 102.5 | −2.08 |
| crystal ($I$-4) [exp][19,20] | 1.030 | 2.019 | 2.484 | 103.1 | |

[a]To compare the association energies of $LiNH_2$ monomers with the solid, the calculations were carried out at the same levels of theory. The calculated results are compared with the available experimental values [exp]. *A.E. = Association energy per $LiNH_2$ = $[E(LiNH_2)_n - nE(LiNH_2\text{−monomer})]/n$. See Supporting Information, Table S1, for absolute total electronic energies of various $LiNH_2$ structures.

**$LiNH_2$ at $P$ = 1 atm.** The $T$ = 298 K, $P$ = 1 atm phase of $LiNH_2$ is experimentally known.[19,20] $LiNH_2$ crystallizes in the body-centered tetragonal space group $I\bar{4}$, a structure (Figure 2)

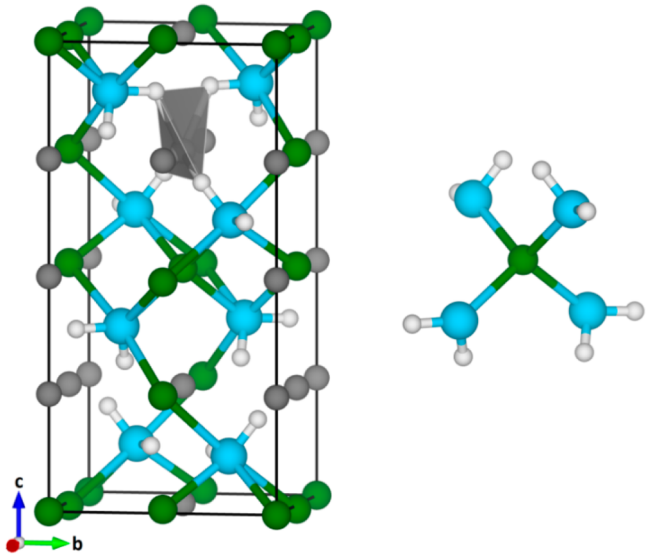


**Figure 2.** Crystal structure of $I\bar{4}$ $LiNH_2$ at 1 atm in its conventional tetragonal unit cell and its tetrahedrally coordinated $Li(NH_2)_4$ unit. N, Li, H, and tetrahedral holes are represented by large (light-sky blue), medium (green), small (white), and medium (gray) spheres, respectively. One irregular tetrahedral hole with nearest-neighbor hydrogen connections ($\square H_4$) is shown in a polyhedral representation.

in which the Li ions are surrounded by $NH_2^-$ groups in a regular and slightly distorted tetrahedral arrangement. Each nitrogen atom is coordinated by four lithiums in addition to its two bonded hydrogens (extracted from the structure in Figure 2, right). We proceeded to calibrate our computations (the theoretical methodology we use is described in the Appendix) on this structure. The optimized lattice parameters ($a$ = $b$ = 5.00 and $c$ = 10.35 Å) and internuclear separations (see Table 1) are in good agreement with experimental values. The N−H bond length is very close to that computed for a molecular $LiNH_2$−monomer (N−H = 1.02 Å, Figure 1) and dimer (N−H = 1.03 Å, Figure 1). The H−N−H angle (103°) in an $NH_2^-$ unit of $LiNH_2$ solid, monomer, and dimer is about the same, but the Li−N distance and the configuration at each N is quite different; the $LiNH_2$ monomer is planar, while the diborane-like dimer and solid are quite pyramidal at each N. (See the Supporting Information, Figure S1, to this article for a more detailed analysis, showing a histogram for the various bond lengths of the $LiNH_2$ crystal structure.)

The $I\bar{4}$ phase is three-dimensionally connected, but from another perspective, it can also be viewed as composed of bilayers of $NH_2^-$ groups intercalated between two-dimensional rafts of lithium cations (see Supporting Information, Figure S2). These rafts are in turn connected by Li ions. The structure has distorted tetrahedral holes, one of which is shown in Figure 2. The holes are defined by hydrogen atoms ($\square H_4$), with average edge length 1.55 Å (average tetrahedron volume, 1.47 Å$^3$). The layer-like structure and quasi-molecular nature of solid $LiNH_2$, together with the presence of some holes or cavities, makes one think there might be pathways for possible phase transitions in $LiNH_2$ at relatively low pressures.

**$LiNH_2$ Phases up to 40 GPa.** The literature contains an *in situ* high-pressure Raman spectroscopic study of $LiNH_2$ up to


dx.doi.org/10.1021/jp3078387 | J. Phys. Chem. A 2012, 116, 10027−10036

25 GPa and $T$ = 298 K.[21] In this work, a phase transition was observed at about 12 GPa. The crystal structure of the resulting phase was not obtained. However, in very recent high pressure (up to 28 GPa) synchrotron X-ray diffraction measurements coupled with theoretical calculations, a new phase for $LiNH_2$ at 12 GPa was proposed.[22] It is monoclinic, space group $P2_1$. We will discuss here, in our systematic structure search, four other structure types: (i) $NaNH_2$ (*Fddd*), (ii) $BaS_3$ or $AgDyTe_2$-type ($P\bar{4}2_1m$), (iii) $LiClO_2$ ($P4_2/ncm$), and (iv) an orthorhombic phase ($P2_12_12_1$). These emerged as enthalpically and dynamically stable ground state structures around 6, 11, 13, and 46 GPa, respectively. The pressure versus enthalpy curves for the stable structures as well as some potentially metastable ones are shown in Figure 3 up to 60 GPa (see Supporting

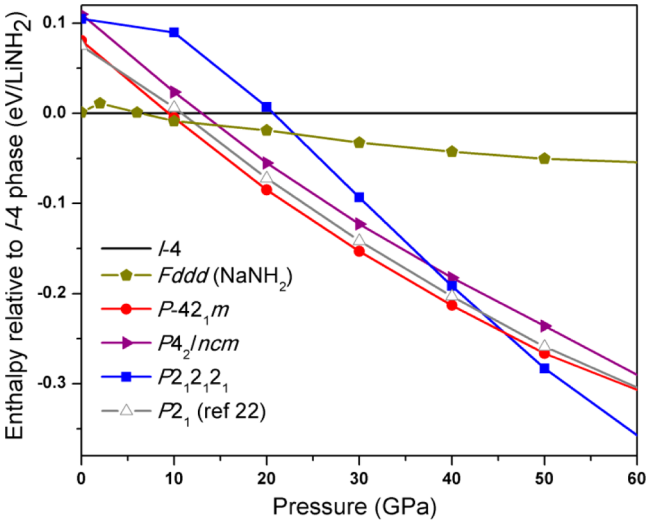


**Figure 3.** Enthalpies of selected ground state crystal structures of $LiNH_2$ relative to $I\bar{4}$ phase. The enthalpies are for ground state static structures without zero-point motion.

Information, Figure S3, for more enthalpies of structures omitted from Figure 3, Figure S4 for phonon density of states of the stable phases, Figure S5 for pressure−volume data, and Figure S15 for calculated XRD patterns).

The first structure to emerge (at 6 GPa), which is competitive with the $I\bar{4}$ $P$ = 1 atm phase, was found by us on trying a $NaNH_2$ structure. This *Fddd* structure (with $Z$ = 16), while not shown here, has a very similar local chemical environment to that of the $I\bar{4}$ phase: each lithium atom is tetrahedrally surrounded by $NH_2^-$ units, and nitrogen is 6-fold (4Li + 2H) coordinated. The two structures mainly differ in their nitrogen sublattices; the $I\bar{4}$ phase has a distorted fcc nitrogen sublattice, and the $NaNH_2$ structure is bct (see Supporting Information, Figure S6, for *Fddd* and $I\bar{4}$ phase structural comparisons). The enthalpy difference between these two phases is not significant throughout their stability region, between 6 to 11 GPa (Figure 3). The *Fddd* structure is dynamically stable, as is the $I\bar{4}$ phase. We suggest that in this pressure regime one may well find one or the other, or both structures, depending on the method of preparation of $LiNH_2$.

At pressures above ∼11 GPa, two new ground state phases ($P\bar{4}2_1m$, $Z$ = 2, and $P4_2/ncm$, $Z$ = 4) become more stable relative to the *Fddd* phase. The $P4_2/ncm$ phase is always higher in enthalpy than the $P\bar{4}2_1m$ phase (0.02 eV/f.u. at 20 GPa, Figure 3). Both structures are dynamically stable. The structures both contain two-dimensional (2D) lithium square sublattices with interpenetrating $NH_2^-$ bilayers, as shown in Figure 4. The distance between nearest neighbor Li atoms in

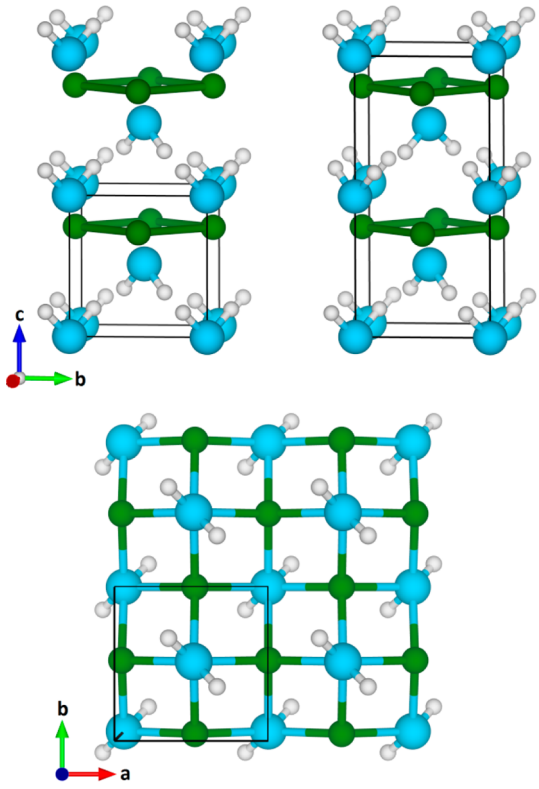


**Figure 4.** Crystal structures of $P\bar{4}2_1m$ and $P4_2/ncm$ (top) phases of $LiNH_2$ at 20 GPa ($V_0/V$ = 1.5). At bottom, a $P\bar{4}2_1m$ 2 × 2 two-dimensional layer of Li−$NH_2$ is shown in a view along the *c*-axis. Notice the nearest neighbor $NH_2^-$ units capped alternatively above and below the 2D lithium square sublattice. The Li−Li connections shown here are only a guide to the eye for seeing the geometry of the Li-sublattice. Structures $P\bar{4}2_1m$ and $P4_2/ncm$ have different space groups in different pressure intervals.[23] See Supporting Information, Figure S7, for high pressure structures of $P\bar{4}2_1m$ and $P4_2/ncm$.

$P\bar{4}2_1m$ and $P4_2/ncm$ $LiNH_2$ is 2.46 and 2.44 Å at 20 GPa. These distances are similar to the Li−Li distance in NaCl-type LiH (2.54 Å, 20 GPa). The two phases ($P\bar{4}2_1m$ and $P4_2/ncm$) are differentiated only by the stacking arrangement of amide anions. In $P\bar{4}2_1m$, the amide anions are stacked in eclipsed fashion, and in $P4_2/ncm$, they are staggered, doubling the unit cell.[23] We note that the $P2_1$ $LiNH_2$ structure proposed by Huang et al.[22] as a new phase for $LiNH_2$ above 10 GPa is a distorted variant of $P\bar{4}2_1m$ or $P4_2/ncm$ structures. This $P2_1$ $LiNH_2$ structure is enthalpically degenerate with respect to $P\bar{4}2_1m$ structure. At 20 GPa, the $P2_1$ structure is 0.013 eV/$LiNH_2$ higher in enthalpy than $P\bar{4}2_1m$ (see Figure 3).

The coordination of lithium and nitrogen in these intermediate pressure phases is similar to that in the $I\bar{4}$ phase (see Supporting Information, Figure S8, for distance histogram). These phases can also be visualized as quasi-two-dimensional Li−N−H layers spread across the *ab*-plane, with $NH_2^-$ units coordinated to the lithium square sublattice forming an extended $LiNH_2$ network as shown in Figure 4, right. The closest distance between Li and N in $P\bar{4}2_1m$ and $P4_2/ncm$ is 1.97 and 1.98 Å at 20 GPa, which is comparable to that of the Li−N distance in $\beta$-$Li_3N$ (1.92 Å, 20 GPa, $V_0/V$ = 1.22).


dx.doi.org/10.1021/jp3078387 | J. Phys. Chem. A 2012, 116, 10027−10036

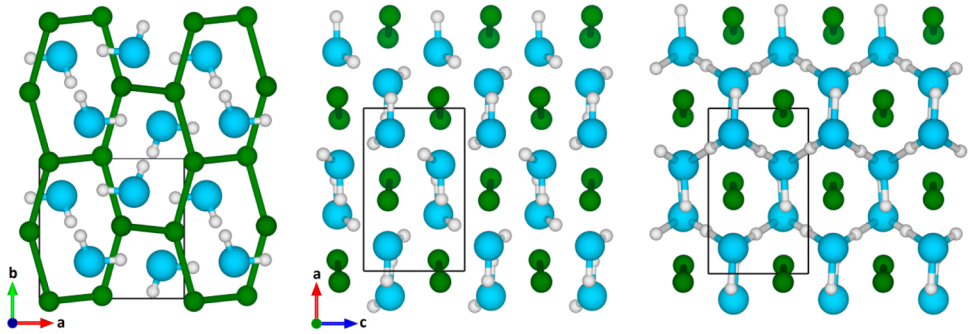


**Figure 5.** Ground state crystal structure of $LiNH_2$ $P2_12_12_1$ phase shown in top view of *ab*- (left) and *ac*-planes (middle) at 60 GPa ($V_0/V$ = 2.48). The structure at 360 GPa ($V_0/V$ = 4.25) with its N···H···N hydrogen bonds is shown at right. Note, for clarity in visualizing the N−H···N or N···H···N hydrogen bonds, some of the Li−Li internuclear connections are not shown in the middle and right figures.

These intermediate pressure $LiNH_2$ phases are stabilized by Li−$NH_2$ coordination, much as the $LiNH_2$ dimers or oligomers or the $P$ = 1 atm $LiNH_2$ solid structure are. As we will see, further stabilization may be present from hydrogen-bond formation in $NH_2^-$ bilayers or between Li−N−$H_2$ layers.

**Phases Above 40 GPa.** At ∼46 GPa, a new phase emerges (see Figure 3) in $LiNH_2$, its lithium network different from lower pressure phases but still containing discrete $NH_2^-$ units (N−H = 1.02 Å at 46 GPa). This orthorhombic $P2_12_12_1$ space group structure with $Z$ = 4, shown in Figure 5, has a distorted adamantane-like lithium sublattice with Li−Li distance of 2.30 Å at 60 GPa, which is similar to the Li−Li distance in LiH (2.32 Å, 60 GPa) but somewhat longer than in elemental Li *CI*16 (1.95 Å, 60 GPa). The $NH_2^-$ units are running along the *c*-axis through the Li hexagonal channels. The N atoms form a distorted hcp sublattice similar to that found in phase IV of $NH_3$ ($P2_12_12_1$).

As pressure increases, one would expect an increase in coordination numbers of the atoms in any structure. Indeed, in the $P2_12_12_1$ phase, lithium now has six nearby $NH_2^-$ units (Li−N = 1.86 Å, 60 GPa) and nitrogen is 8-fold-coordinated (6Li + 2H); see Supporting Information, Figure S9, for distance histogram of $P2_12_12_1$ at 60 GPa. As we shall see, the $NH_2^-$ units running along the Li-hexagonal channels feature hydrogen bonds (N−H···N) between the nearest neighbor $NH_2^-$ units.

The $P2_12_12_1$ phase remains stable in our calculations beyond 100 GPa (Figure 6). Structure searches up to 360 GPa repeatedly found this structure and no other more stable phases. The $P2_12_12_1$ structures we found all feature an interesting local atomic ordering, infinite zigzag $NH_2^-$ polymer chains, with $NH_2$ molecular identity increasingly lost, and an approach to a symmetrical ···(H)N···H···N(H)···H··· hydrogen bonding network, where one of the hydrogen atoms of what was originally an amide unit bridges to a neighboring, initially unbound, nitrogen, as shown in Figure.5, right. We will discuss this fascinating feature of the high pressure phases in some detail below.

At pressures above 260 GPa, four new phases, *Cc*, $Pna2_1$, *Pnma*, and $Pmc2_1$ were also found, all with the feature of infinite zigzag $NH_2^-$ polymer chains (Figure 6). The *Cc*, $Pna2_1$, and *Pnma* structures were found in an XtalOpt search, while the $Pmc2_1$ phase came from exploring $LiNH_2$ analogues to high pressure $H_2O$-ices.[10] A search based on high pressure ionic $NH_3$ phases[7] did not lead to any new structures.

Three of the above-cited new structural types, while dynamically stable in a certain pressure range, are consistently higher in enthalpy than the $P2_12_12_1$ structure (up to 500 GPa).

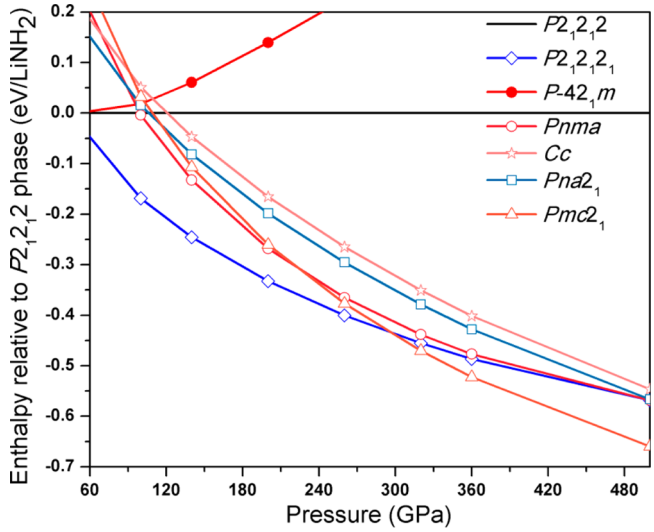


**Figure 6.** Ground state enthalpies of selected (lower enthalpy) ground state crystal structures of $LiNH_2$ relative to the $P2_12_12$ phase. Note that the reference structure ($P2_12_12$) differs from that in Figure 3. Also, the pressure range here is ≥60 GPa, whereas in Figure 3, it is ≤60 GPa. Structures with open symbols are the ones approaching a symmetrical N···H···N hydrogen bonding network. The enthalpies are for static structures without zero-point motion. See Supporting Information, Figure S3 for details on high enthalpy phases.

We give some details of these phases in the Supporting Information, Figure S10. The $Pmc2_1$ structure surpasses $P2_12_12_1$ in stability above 280 GPa (see Figure 6). Let us then look in more detail at the calculated $P2_12_12_1$ and $Pmc2_1$ phases.

**Infinite Hydrogen Bonded Polymer.** The striking feature of the stable high-pressure phases is the infinite zigzag ···(H)N···H···N(H)···H··· hydrogen bonding polymer network, and its approach to symmetrization. Two representative structures, one slightly asymmetrical ($P2_12_12_1$), one symmetrized ($Pmc2_1$), are shown in Figure 7. The bond lengths of intramolecular N−H and intermolecular N···H bonds in the amide anion zigzag network of $P2_12_12_1$ $LiNH_2$ at 360 GPa are calculated to be 1.04 and 1.27 Å, respectively. They become symmetric only at ∼500 GPa ($V_0/V$ = 4.8). The $Pmc2_1$ structure, the competitive phase at high pressures, contains symmetric N···H···N hydrogen bonds from the pressure at which it first becomes stable, 280 GPa, where the N···H bond length is 1.17 Å.

It is clear from the high pressure (>280 GPa) $LiNH_2$ structures that the formation of infinite zigzag $NH_2^-$ polymeric


dx.doi.org/10.1021/jp3078387 | J. Phys. Chem. A 2012, 116, 10027−10036

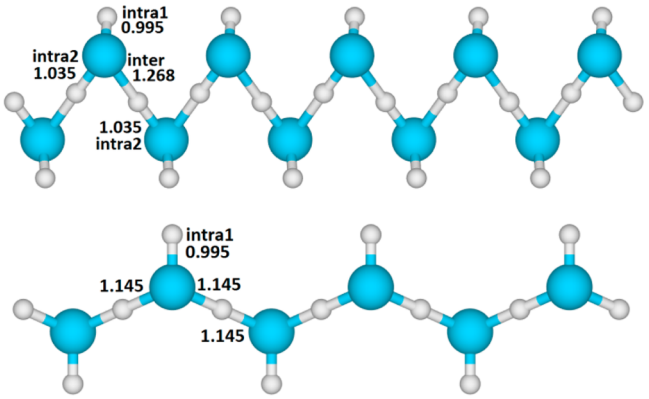


**Figure 7.** Formation of infinite zigzag $NH_2^-$ polymeric chains in $P2_12_12_1$ (above) and $Pmc2_1$ (below) at 360 GPa. Various intra-N−H and inter-N···H bond lengths around N centers are given in Å.

networks, one H involved in (eventually symmetrical) hydrogen bonding, the other not, is the characteristic structural feature of high pressure $LiNH_2$ phases, at least between 280 to 500 GPa. Given the structurally significant formation of hydrogen bonds in the various $LiNH_2$ solids calculated in this pressure range, it makes sense to analyze these in some detail.

It appears that $LiNH_2$ under pressure (up to 20 GPa) has also been explored theoretically by Zhong et al.,[24] who obtained a sequence of phases with increasing pressure that is similar to that found by us, $I\bar{4} \rightarrow Fddd \rightarrow P2_12_12$ or $P\bar{4}2_1m$.

**Hydrogen Bonding in Formation.** The reader is no doubt aware that the origin of hydrogen bonding, a ubiquitous and important phenomenon at $P = 1$ atm, is the subject of much contention. The recent discussion of the IUPAC definition of hydrogen bonding is one piece of evidence of this.[25] This weak bonding has components in it of dispersion forces, of polar/multipole interactions, and of orbital effects, donation from lone pairs of one component to the $\sigma^*$ orbitals of the other. The debate is over the relative weight of each component. This is not the place to enter this contentious discussion, and we focus mainly on the structural manifestations of hydrogen bonding.

A calibration point for the distances involved in N−H···N hydrogen bonding might be ammonia itself, whose melting point is raised significantly due to hydrogen bonding. The dimer of $NH_3$, a simple model for this hydrogen bonding, is held together by some 3.1 kcal/mol.[26] The preferred geometry is slightly nonlinear, easily bent, with N−H 1.02 and N···H 2.47 Å.

In the low pressure $I\bar{4}$ phase, the $NH_2^-$ groups are oriented in such a way that there are no significant direct intermolecular N−H···N contacts between the neighboring $NH_2^-$ groups (see Figure 2). So the possibility for hydrogen bonding in $I\bar{4}$ phase can be neglected. Figure 8a shows the evolution of the intramolecular N−H distances in this structure. As the pressure is increased, this phase is superseded by *Fddd*, which also shows no signs of hydrogen bonding.

The first indication of incipient N−H···N interaction is found in the $P\bar{4}2_1m$ and $P2_12_12_1$ predicted phases; the nearest neighbor $NH_2^-$ groups' molecular planes are orthogonal to each other in $P\bar{4}2_1m$ (at 20 GPa) and somewhat tilted (~65° at 60 GPa) in $P2_12_12_1$, which facilitates direct N−H···N internuclear contacts (see Figures 4 and 5). The closest intermolecular N···H distance in $P\bar{4}2_1m$ (20 GPa) and $P2_12_12_1$ (60 GPa) are 1.96 and 1.77 Å, respectively (see Figure 8).

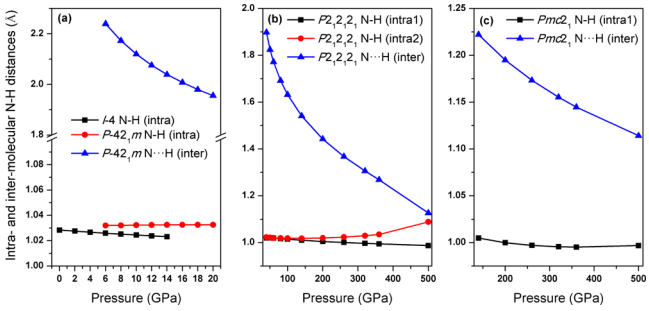


**Figure 8.** Evolution of N−H and N···H distances in (a) $I\bar{4}$ and $P\bar{4}2_1m$, (b) $P2_12_12_1$, and (c) $Pmc2_1$ $LiNH_2$ structures under pressure. The two N−H(intra) bond lengths in $NH_2^-$ (see text and Figure 7 for definition) of $I\bar{4}$ are the same throughout the pressure range shown here. So, only one N−H(intra) distance in the $I\bar{4}$ structure is given. Similarly, the two N−H bonds of an $NH_2^-$ unit in $P\bar{4}2_1m$ are the same and also the two N···H hydrogen bond distances. The N−H (intra2) and N···H intermolecular distances in $Pmc2_1$ are also the same. Therefore, one representative distance is given in the plot (see text and Figure 7).

The two hydrogens in an $NH_2^-$ unit of the $P\bar{4}2_1m$ structure form an N···H hydrogen bond each with the nearest nitrogen atom of $NH_2^-$, whereas in the $P2_12_12_1$ structure, one hydrogen of $NH_2^-$ form a hydrogen bond with the nearest $NH_2^-$, while the second hydrogen is not significantly involved. The N−H···N bonds are aligned almost linearly (~171°) in the $P\bar{4}2_1m$ and $P2_12_12_1$ phases. These calculated distances and angles are similar to the computed hydrogen bonding distances in the $NH_3$ $P2_12_12_1$ phase at 20 (1.87 Å, 168°) and 60 GPa (1.67 Å, 169°).[7]

The definition of the various NH distances involved in the high pressure phases was given above, but we repeat it in Figure 9 for clarity.

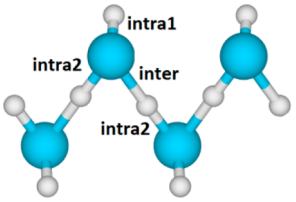


**Figure 9.** Definition of distances in extended ···(H)N···H···N(H)···H structures. N−H(intra1) is the NH bond that remains out of the hydrogen-bonding chain and is short; N−H(intra2) is the shorter NH bond, originally equal to NH(intra1) in $P2_12_12_1$ but lengthening as the hydrogen bonding network forms. The longer N−H bond is the N···H intermolecular hydrogen bond.

At higher pressures, the $P2_12_12_1$ and $Pmc2_1$ structures are the important ones in their ground states. In the first of these structures, at pressures above 150 GPa, the two N−H bond lengths in an $NH_2^-$ group are not the same. The N−H(intra1) bond, not participating in the hydrogen-bonded network, is slightly shortened (see Figures 8b, 7, and 9) with increasing pressure, while the other N−H bond, N−H(intra2), part of the zigzag hydrogen-bonded chain, is relatively elongated. Eventually, at pressures ~500 GPa, the N−H(intra2) and N···H-(inter) hydrogen bonds becomes symmetric (N···H···N, see Figure 8), forming the infinite zigzag ···(H)N···H···N(H)···H polymer network.


dx.doi.org/10.1021/jp3078387 | J. Phys. Chem. A 2012, 116, 10027−10036

The evolution of N−H and N···H distances in $Pmc2_1$ is slightly different from $P2_12_12_1$. The N−H(intra1) distance, that of the N−H bond not involved in hydrogen bonding, does not change with pressure. As a consequence of crystal symmetry in this space group, the N−H(intra2) and N···H(inter) distances are identical. This N···H bond is shortened to some extent (1.22, 140 GPa to 1.11 Å, 500 GPa) as shown in Figure 8c. The Supporting Information (Figure S11) contains an analysis of the hydrogen bonding based on charge density and the electron localization function that also supports the view presented here.

**Enthalpy of N−H···N Symmetrization.** The calculated enthalpy of symmetrization of N−H(intra2) and N···H(inter) bonds is shown in Figure 10. This figure also shows the corresponding equilibrium bond lengths in the favored (asymmetric) structure. The enthalpy of symmetrization is calculated as the enthalpy difference between $P2_12_12_1$ structures with asymmetric and symmetrized N−H(intra2) and N···H-(inter) bonds at constant pressure. The enthalpy of symmetrization is about 0.14 eV/$LiNH_2$ at 200 GPa and decreases with increasing pressure. It is clear from Figure 10 that as the asymmetric N−H···N bond in this phase approaches symmetrization the associated enthalpy for symmetrization approaches zero.

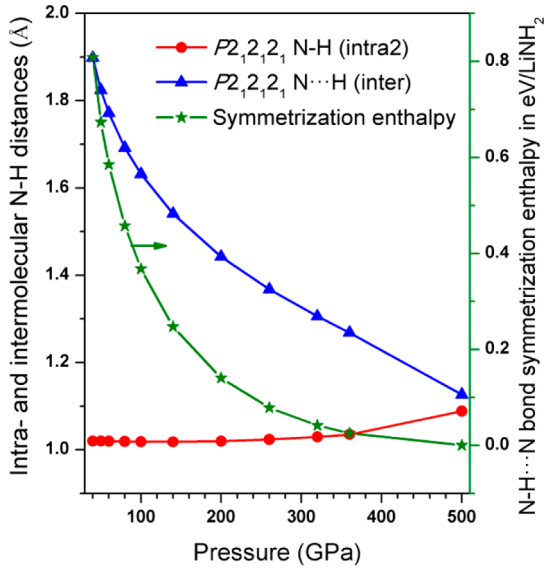


**Figure 10.** Calculated enthalpy of N−H(intra2) and N···H(inter) bond symmetrization in $P2_12_12_1$ structure at constant pressure. The arrow refers to the curve indicated to the scale on the right.

In summary, the $LiNH_2$ structures are characterized at higher pressures by evolving ···(H)N···H···N(H)···H zigzag polymeric chains, in which one NH bond is kept out of the chain, the other loses its connection to one specific nitrogen, and with increasing pressure becomes symmetrically coordinated to two NH groups.

**Evolution of Phonons in $LiNH_2$ with Pressure.** Figure 11, left, shows the computed (in the harmonic approximation) high frequency N−H stretching modes in the $LiNH_2$ $I\bar{4}$ and $P\bar{4}2_1m$ structures, as a function of pressure. For the rest of the phonon spectrum, see the phonon density of states given in the Supporting Information. The calculated N−H stretching frequencies in the $I\bar{4}$ $LiNH_2$ structure at 1 atm (symmetric combination of N−H stretches ∼3360 and asymmetric combination 3430 $cm^{-1}$) are in reasonable agreement with the reported experimental values (3269 and 3332 $cm^{-1}$), especially in their relative order in energy. The existence of several modes of each type is a consequence of several site symmetries in the $Z = 4$ primitive crystal. Both symmetric and asymmetric N−H stretching frequencies increased in our calculations with increasing pressure in the $I\bar{4}$ $LiNH_2$ structure, matching experimental observations of Chellappa et al.,[21] Figure 11, right.

As we discussed above, the ground state of $LiNH_2$ undergoes a possible phase transition at 6 GPa into an *Fddd* structure. The vibrational frequencies in this structure (not shown in Figure 11) increase with increasing pressure as in the $I\bar{4}$ structure. However, in the next structure encountered as the pressure rises, the $P\bar{4}2_1m$ structure found at 11 GPa, the N−H stretching frequencies are lowered by ∼100 $cm^{-1}$ (Figure 11, left). The lowered N−H stretching frequencies in this phase can be attributed to the incipient formation of N−H···N hydrogen bonding in $P\bar{4}2_1m$ $LiNH_2$ structure, as discussed above.

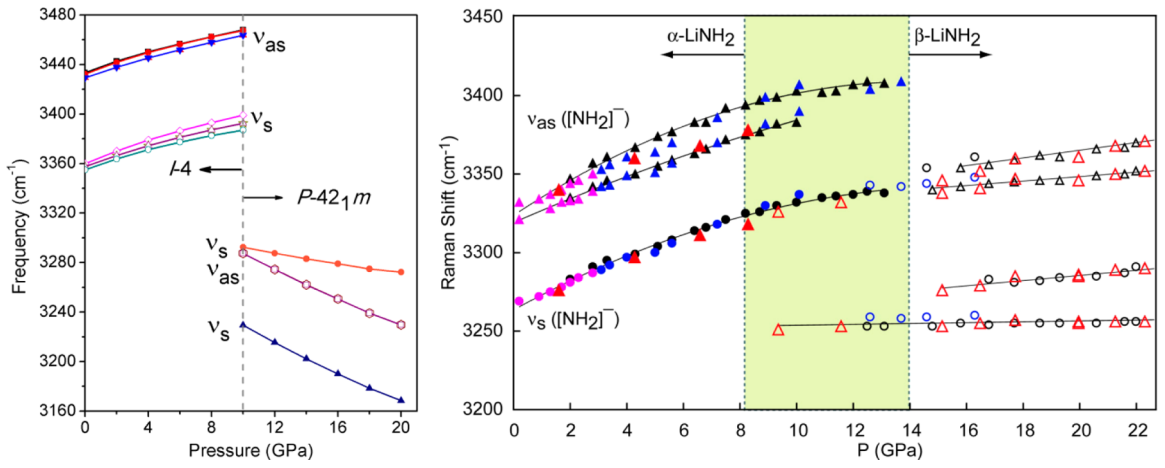


**Figure 11.** Evolution of N−H stretching frequencies in $I\bar{4}$ and $P\bar{4}2_1m$ $LiNH_2$ structures with increasing pressure. The $\nu_s$ and $\nu_{as}$ indicate the symmetric and asymmetric combinations of N−H stretching frequencies, respectively. The $I\bar{4}$ $LiNH_2$ structure contains 4 $LiNH_2$ formula units (16 atoms per primitive unit cell) and hence 8 N−H stretching modes. Similarly, $P\bar{4}2_1m$ $LiNH_2$ has 4 N−H stretching modes as it has 2 formula units (8 atoms per unit cell). The left figure is from our calculations, the right from the measurements of Chellappa et al.[21]


dx.doi.org/10.1021/jp3078387 | J. Phys. Chem. A 2012, 116, 10027−10036

The lowering of N−H stretching frequencies in the $P\bar{4}2_1m$ $LiNH_2$ phase agrees quite well with the experimental N−H stretching modes of $LiNH_2$ above 12 GPa (see Figure 11, right). However, some discrepancies with experiments may be seen. In the calculations, we see a decrease in N−H stretching frequencies with increasing pressure, whereas in experiment, these frequencies are almost constant or increase somewhat with pressure. Furthermore, Chellappa et al. suggest (based on their observation on increased number of lattice modes) that the $LiNH_2$ phase above 12 GPa would be lower in symmetry or might contain more formula units per unit cell ($Z > 8$) in comparison to the $I\bar{4}$ $LiNH_2$ conventional cell ($Z = 8$). These features are not in agreement with our proposed $P\bar{4}2_1m$ ($Z = 2$) or $P4_2/ncm$ ($Z = 4$) $LiNH_2$ structures.

As we go up in pressure, the N−H stretching frequencies in $P2_12_12_1$ $LiNH_2$ structure (favored above 46 GPa) behave differently from the $I\bar{4}$ and $P\bar{4}2_1m$ structures. Some N−H stretching frequencies increase with pressure and some decrease. Because of the diminished symmetry, the $P2_12_12_1$ structure contains multiple N−H stretching modes spanning a large frequency window (3425 to 3247 $cm^{-1}$ at 46 GPa) with increasing pressure. The high energy branches here are at frequencies 3400−3700 $cm^{-1}$, higher than the low pressure phases (see Supporting Information, Figure S12, for N−H stretching frequencies with pressure in $P4_2/ncm$ and $P2_12_12_1$ $LiNH_2$ structures).

**Negative Enthalpies of Formation.** Figure 12 shows the computed enthalpies of formation ($\Delta H_f$) of the stable $LiNH_2$ phases with respect to elemental N, Li, and H in their most probable ground state structures at a given pressure. The computed standard $\Delta H_f$ for $LiNH_2$ $I\bar{4}$ phase is −2.07 eV per formula unit, which is 12% higher than the experimental[27] value (−1.83 eV). It should be noted that the heat of formation in the literature is under standard conditions ($P$ = 1 atm, 298 K), while our calculations are for the ground states, approaching 0 K. We have not attempted an adjustment of the experimental $\Delta H_f$ to 0 K, as we lack heat capacity information for solid $LiNH_2$. Including the zero-point motion of the nuclei within the harmonic approximation improved the agreement with experiment, giving $\Delta H_f$ = 1.73 eV. The increasingly more negative $\Delta H_f$ of $LiNH_2$ structures as the pressure increases clearly indicates that the newly predicted structures are thermodynamically quite stable with respect to their elements.

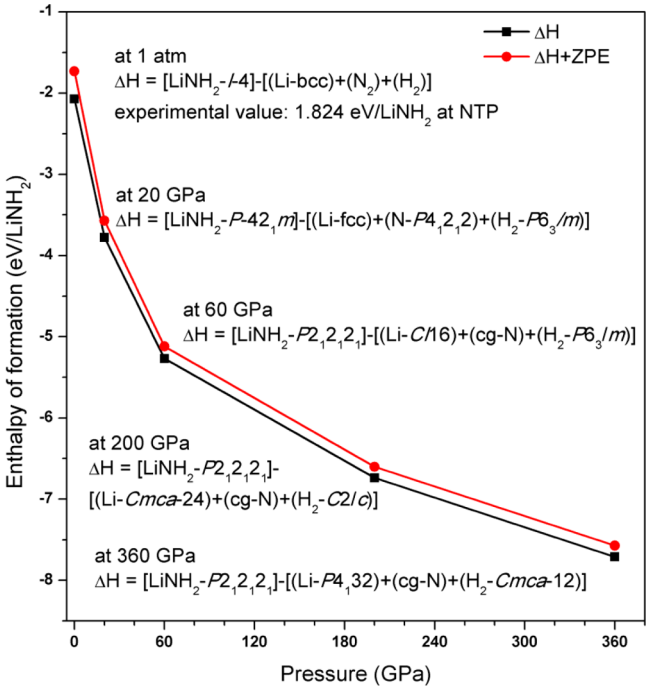


**Figure 12.** Computed enthalpies of formation ($\Delta H_f$) of the most stable $LiNH_2$ phases with and without zero-point energies. The reactions used to estimate the $\Delta H$ values at a given pressure are displayed closer to the respective data points.

**Amide Ordering and Lithium Distortions.** The $LiNH_2$ structures we find at intermediate pressures are layer-like; they contain anionic amide molecular groups in-between layers of lithium cations (see Figure 4). The amide groups are certainly ionically bound to the Li sublattice. In addition to this ionic bonding, above 10 GPa, the amide molecules are also held together by intermolecular hydrogen bonding. These structural predictions (see Figures 4 and 5) lead to another perspective; in these geometries, one might profitably think of rotations of the amide groups around their molecular pseudo $C_2$ axis or displacive distortions in the Li layers. The calculated rotational barrier for an $NH_2$ group is about 0.62 and 1.17 eV/$NH_2$ in the $I\bar{4}$ and $P\bar{4}2_1m$ $LiNH_2$ structure at 1 atm and 20 GPa, respectively. See the Supporting Information for more details on calculations of the energy barriers. The large barrier to amide rotation in the $P\bar{4}2_1m$ $LiNH_2$ structure arises from breaking the N−H···N hydrogen bonding between the $NH_2$ groups that are orthogonal to each other (see Figures 4 and S13, Supporting Information) and also the sterical contacts that arise between $NH_2$ groups on rotation.

We also wanted to see how much energy might be involved in lithium sublattice motions. For this purpose, we followed low frequency phonons that can be identified as mainly belonging to lithium sublattice motion in the relatively less complex $P\bar{4}2_1m$ $LiNH_2$ crystal structure. We find that the Li square lattice has two characteristic low frequency phonon modes (around 400 $cm^{-1}$ at 20 GPa), namely, a puckering and a slip mode. The two modes are shown below in Figure 13.

We followed these Li phonon modes and found that the energy needed to displace Li cations from planar to puckered sheets is ∼0.10 eV/$LiNH_2$, and, for the slip mode, 0.14 eV/$LiNH_2$. The geometries optimized within the constraints of the above phonon modes are given in the Supporting Information, Figure S14.

The high barrier for $NH_2$ rotations in $P\bar{4}2_1m$ $LiNH_2$ structure is an indication of orientational ordering, but the relatively low barriers for Li distortions could lead to displacive structural phase transitions[28] or lithium sublattice melting at high temperature and pressure. The slip-mode barrier calculated is less than 80% of the energy of the zero-point motion in the $P\bar{4}2_1m$ $LiNH_2$ structure at 20 GPa (ZPE = 0.8 eV/$LiNH_2$, the large ZPE is mainly due to the strong N−H stretching frequencies). The lithium slipping motion is especially relevant, as it leads to a sublattice rearrangement. However, it will take


dx.doi.org/10.1021/jp3078387 | J. Phys. Chem. A 2012, 116, 10027−10036

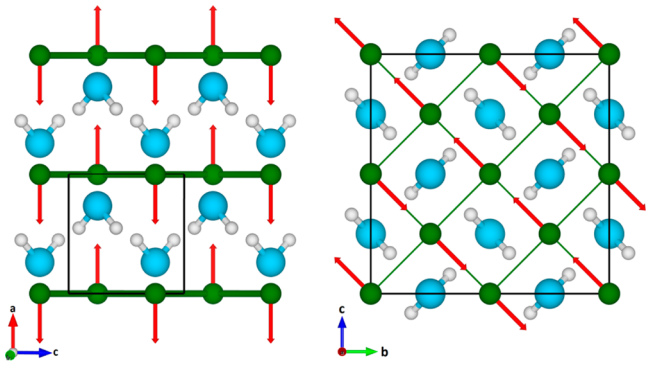

**Figure 13.** Two low frequency phonon modes of the Li sublattice in $P\bar{4}2_1m$ at 20 GPa.

molecular dynamics and an examination of partial static structure factors to sort this out. We intend to undertake this in a subsequent study.

**Increasingly Insulating in Intermediate Pressure Range.** The calculated electronic density of states (DOS) of $LiNH_2$ $I\bar{4}$ at 1 atm is shown in Figure 14a. The narrow bands, with large gaps between them, are characteristic of a molecular solid. VASP decompositions of the density of states are only indicative, but they give us an idea of the parentage (by atom and orbital) of the various bands. Given the polarity $Li^+NH_2^-$, we expect two NH bonding bands and two NH lone pairs as the highest occupied bands, then a substantial gap to a mainly $Li^+$ conduction band, mixed with NH $\sigma^*$ orbitals. This is what is observed. The computed charges,[29] Li(0.84), N(−1.48), and H(0.32) suggest that the $LiNH_2$ is therefore dominantly ionic in nature.

The DOSs of the high pressure $LiNH_2$ phases ($P\bar{4}2_1m$ and $P2_12_12_1$ at 20 and 60 GPa, respectively) are similar to that of $LiNH_2$ $I\bar{4}$ at 1 atm, except the filled states become broader and begin to overlap with increasing pressure, as shown in Figure 14a. The calculated band gaps of $LiNH_2$ $I\bar{4}$, $P\bar{4}2_1m$, and $P2_12_12_1$ phases at 0, 20, and 60 GPa (in regions of the stability of these phases) are 3.1, 5.4, and 5.2 eV, respectively.

Figure 14b shows the evolution of the band gaps of the various phases with pressure. Remarkably, the band gaps of all the phases initially rise with pressure, up to around 60 GPa. Above that pressure, the band gaps of the less stable phases decrease, a common feature, but the band gaps of the most stable high pressure phases, $P2_12_12_1$ and $Pmc2_1$, continue to increase, stabilizing at ∼5.5 eV, with no sign of gap closure at 500 GPa. Calculations not reported in detail here indicate that $P2_12_12_1$ and $Pmc2_1$ will become metallic only around 4 and 5 TPa (11 and 9.7 fold compression), respectively. This feature is also found in $H_2O$-ices[10] and $Li_3N$[30] under pressure. We note that DFT underestimates the band gaps, so the values cited should be considered as the lower limit of the metallization pressures. The calculated charges of $LiNH_2$ ($P2_12_12_1$ and $Pmc2_1$) at 360 GPa are Li(0.68, 0.68), N(−1.54, −1.57), and H(0.43, 0.46), indicating that the structures are pretty much ionic. Electron transfer and chemical bonding burn deep holes in the electronic structure of these phases, holes which persist to extremely high pressures.

A comparison with ammonia is in order. Considering the *Pnma* structure of $NH_3$ as the most stable phase under pressure studied so far,[7] our calculations show that the *Pnma* $NH_3$ structure become metallic around 700 GPa, which is much lower than the metallization pressures of $LiNH_2$ (5 TPa), $H_2O$-ices (4.8 TPa), and $Li_3N$ (8 TPa). Though the high pressure $LiNH_2$ structures with N−H···N and N···H···N hydrogen bonding are structurally similar to high pressure $NH_3$ and $H_2O$-ices, the electronic properties are much closer to $H_2O$-ices.

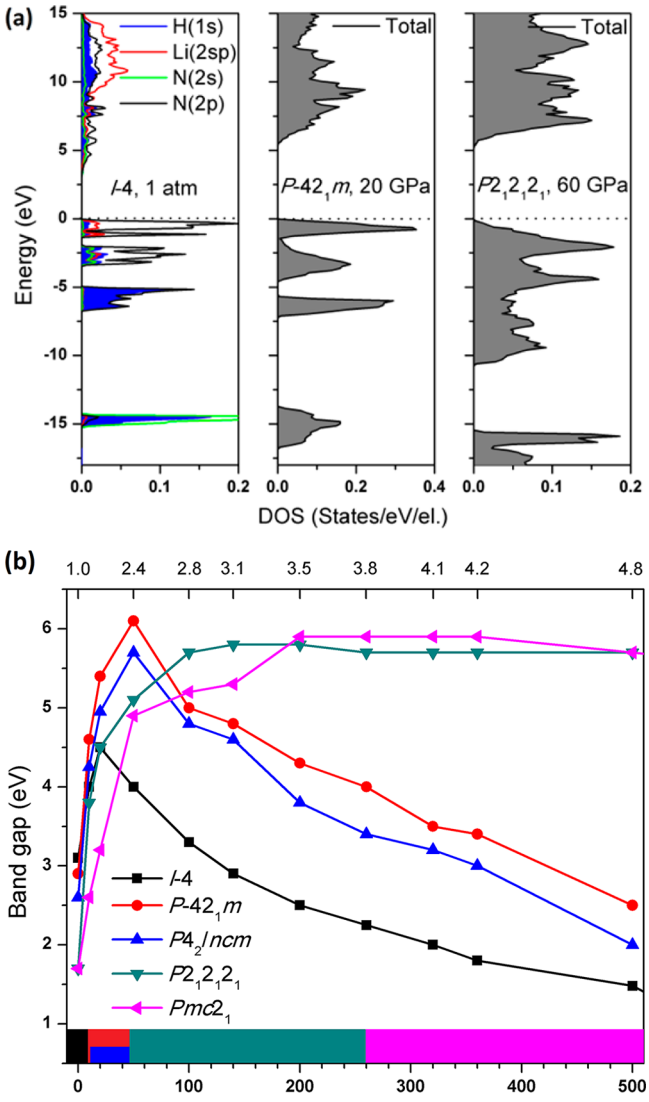


**Figure 14.** (a) Electronic density of states (DOS) of $I\bar{4}$, $P\bar{4}2_1m$, and $P2_12_12_1$ at 1 atm, 20 GPa, and 60 GPa, respectively, and (b) the evolution of band gaps with pressure. The volume compression of the $P2_12_12_1$ structure is shown on the upper horizontal axis. The colored barcode just above the pressure axis indicates the region of a particular $LiNH_2$ phase stability, the color in the barcode matches the color used to represent the $LiNH_2$ phases in the legend.

## CONCLUSIONS

As part of a general exploration of the Li/N/H system, we have examined the ground state structures and bonding in $LiNH_2$ under pressure. We begin by summarizing the state of knowledge of molecular $LiNH_2$ monomers and dimers, and then move on to the $P$ = 1 atm $LiNH_2$ structure, which is well-reproduced by theory. There may be two competing $LiNH_2$ phases at low pressures, with a predicted transition around 6 GPa to an *Fddd* phase. At 11 and 13 GPa, two new phases emerge $P\bar{4}2_1m$, $Z$ = 2, and $P4_2/ncm$, $Z$ = 4, respectively. Both feature square networks of Li between which $NH_2^-$ units are located. There is a possibility of Li sublattice melting in these


dx.doi.org/10.1021/jp3078387 | J. Phys. Chem. A 2012, 116, 10027−10036

structures. At ∼46 GPa, a new phase $P2_12_12_1$ takes over and is stable over a wide pressure region, 46 to 280 GPa. Above 280 GPa, the $Pmc2_1$ phase is the predicted high pressure phase.

A striking structural feature of the high pressure phases of $LiNH_2$ is the presence in their structures of ···(H)N···H···N-(H)···H zigzag polymeric chains, in which one NH bond is kept out of the chain. The other hydrogen is therefore no longer bonded to one specific nitrogen and, with increasing pressure, becomes symmetrically coordinated to two NH groups. Similarities and differences with $H_2O$ and $NH_3$ at high pressures are examined; the predicted structures remain insulating over a wide pressure range.

## APPENDIX

### Theoretical Methodology

Evolutionary structure search algorithms as implemented in the XtalOpt program[31] were used to generate the structural candidates. The ground state enthalpies were obtained using density functional theory (DFT) as implemented in the Vienna *ab initio* Simulation Package (VASP).[32] The generalized gradient approximation of Perdew−Burke−Enzerof[33] was used as the energy functional in our calculations; the electron−ion interaction was treated with the Projector Augmented Wave (PAW) method.[34,35] The PAW potentials represent the valence electrons of Li ($1s^2$, $2s^1$), N ($2s^2$, $2p^3$), and H ($1s^1$). A plane-wave basis set cutoff of 650 eV and self-consistent field tolerance of $0.1 \times 10^{-6}$ eV/atom was set. The Brillouin zone was sampled on a grid of spacing $2\pi \times 0.04$ Å$^{-1}$. With these settings, the structures were fully relaxed until the forces on atoms were less than $10^{-3}$ eV/Å.

Ground state structure searches were carried out at pressures of 1 atm and 10, 100, 260, and 360 GPa with two and four $LiNH_2$ formula units (Z) per unit cell. The structure search was assumed to be complete when we did not find new low enthalpy structures at a given pressure. Some of the low enthalpy structures obtained from previous generations in an evolutionary process were used as seed structures for the next generations. As we have seen, the structures generated by XtalOpt at high pressures are similar to those of high pressure $NH_3$ and $H_2O$-ices. We have also constructed $LiNH_2$ structures by substituting Li for $NH_4^+$ in high pressure ionic structures of $NH_3$ and by filling holes of high pressure $H_2O$-ices by Li atoms, substituting O by N. We also have optimized $LiNH_2$ structures in $NaNH_2$ (*Fddd*) and $KNH_2$ ($P2_1/m$) structure-types. The low enthalpy ground state structures thus obtained are tested for their dynamical stability by computing phonons, using the PHONOPY program.[36] The real space force constants of the super-cells are calculated in the framework of density functional perturbation theory (DFPT)[37] as implemented in VASP.

## ASSOCIATED CONTENT

### Supporting Information

Presented is a table of absolute and association energies of $LiNH_2$ monomer, dimer, trimer, and $I\bar{4}$ crystal structures. Internuclear distance histograms of $I\bar{4}$, $P\bar{4}2_1m$, and $P2_12_12_1$ $LiNH_2$ structures. The $I\bar{4}$ $LiNH_2$ crystal structure in different views. Enthalpies of the ground state crystal structures and phonon density of states of various $LiNH_2$ phases. Calculated pressure−volume curves for the stable $LiNH_2$ phases. The $LiNH_2$ $I\bar{4}$ and *Fddd* structural comparisons. The $P\bar{4}2_1m$ and $P4_2/ncm$ $LiNH_2$ crystal structures above 100 GPa. The $NH_2$ anion zigzag chains in various $LiNH_2$ phases. Charge density and ELF analysis of $LiNH_2$ structures. Evolution of N−H stretching frequencies with pressure. Calculations of the energy barriers in $LiNH_2$ structures. Optimized crystallographic information of various $LiNH_2$ crystal structures. Calculated XRD patterns of $LiNH_2$ phases. This material is available free of charge via the Internet at http://pubs.acs.org.

## AUTHOR INFORMATION

### Corresponding Author

*E-mail: rh34@cornell.edu.

### Notes

The authors declare no competing financial interest.

## ACKNOWLEDGMENTS

We acknowledge Andreas Hermann for providing the high pressure water crystal structure coordinates. Our work at Cornell was supported by the National Science Foundation, through research grant CHE-0910623 and Efree (an Energy Frontier Research Center funded by the Department of Energy (Award Number DESC0001057 at Cornell)). Computational resources provided in part by Efree, also by the XSEDE network (provided by the National Center for Supercomputer Applications through Grant TG-DMR060055N) and by Cornell's NanoScale Facility (supported by the National Science Foundation through Grant ECS-0335765) are gratefully acknowledged.

## REFERENCES

(1) Maynard-Casely, H. E. M.; Bull, C. L.; Guthrie, M.; Loa, I.; McMahon, M. I.; Gregoryanz, E.; Nelmes, R. J.; Loveday, J. S. *J. Chem. Phys.* **2010**, *133*, 064504.

(2) Chen, P.-N.; Zha, C.-S.; Chen, X.-J.; Shu, J.; Hemley, R. J.; Mao, H. K. *Phys. Rev. B* **2011**, *84*, 104110.

(3) Dreele, R. B. V.; Hanson, R. C. *Acta Crystallogr., Sect. C: Cryst. Struct. Commun.* **1984**, *C40*, 1635−1638.

(4) Datchi, F.; Ninet, S.; Gauthier, M.; Saitta, A. M.; Canny, B.; Decremps, F. *Phys. Rev. B* **2006**, *73*, 174111.

(5) Benedetti, L. R.; Nguyen, J. H.; Caldwell, W. A.; Liu, H. J.; Kruger, M.; Jeanloz, R. *Science* **1999**, *286*, 100−102.

(6) The decomposition of methane at high pressure is the subject of some discussion in the literature. For example, see, (a) Ancilotto, F.; Chiarotti, G. L.; Scandolo, S.; Tosatti, E. *Science* **1997**, *275*, 1288−1290. (b) Gao, G.; Oganov, A. R.; Ma, Y.; Wang, H.; Li, P.; Li, Y.; Iitaka, T.; Zou, G. *J. Chem. Phys.* **2010**, *133*, 144508. (c) Spanua, L.; Donadioa, D.; Hohlc, D.; Schwegler, E.; Gallia, G. *Proc. Natl. Acad. Sci. U.S.A.* **2011**, *108*, 6843−6846. Sun, L. L.; Yi, W.; Wang, L.; Shu, J. F.; Sinogeikin, S.; Meng, Y.; Shen, G. Y.; Bai, L. G.; Li, Y. C.; Liu, J.; Mao, H. K.; Mao, W. L. *Chem. Phys. Lett.* **2009**, *473*, 72−74.

(7) Pickard, C. J.; Needs, R. J. *Nat. Mater.* **2008**, *7*, 775−779.

(8) Goncharov, A. F.; Struzhkin, V. V.; Mao, H. K.; Hemley, R. J. *Phys. Rev. Lett.* **1999**, *83*, 1998−2001.

(9) Pruzan, P.; Chervin, J. C.; Wolanin, E.; Canny, B.; Gauthier, M.; Hanfland, M. *J. Raman Spectrosc.* **2003**, *34*, 591−610.

(10) Hermann, A.; Ashcroft, N. W.; Hoffmann, R. *Proc. Natl. Acad. Sci. U.S.A.* **2012**, *109*, 745−750.

(11) Aoki, K.; Katoh, E.; Yamawaki, H.; Sakashita, M.; Fujihisa, H. *Phys. B* **1999**, *265*, 83−86.

(12) Katoh, E.; Yamawaki, H.; Fujihisa, H.; Sakashita, M.; Aoki, K. *Phys. Rev. B* **1999**, *59*, 11244−11250.

(13) Gauthier, M.; Pruzan, P.; Chervin, J. C.; Besson, J. M. *Phys. Rev. B* **1988**, *37*, 2102−2115.

(14) Grotjahn, D. B.; Sheridan, P. M.; Al Jihad, I.; Ziurys, L. M. *J. Am. Chem. Soc.* **2001**, *123*, 5489−5494.

(15) Rutherford, J. L.; Collum, D. B. *J. Am. Chem. Soc.* **1999**, *121*, 10198−10202.

(16) Mulvey, R. E. *Chem. Soc. Rev.* **1998**, *27*, 339−346.

(17) Sapse, A.-M.; Kaufmann, E.; Schleyer, P. v. R.; Gleiter, R. *Inorg. Chem.* **1984**, *23*, 1569−1574.
(18) Donald, K. J.; Hoffmann, R. *J. Am. Chem. Soc.* **2006**, *128*, 11236−11249.
(19) Yang, J. B.; Zhou, X. D.; Cai, Q.; James, W. J.; Yelon, W. B. *Appl. Phys. Lett.* **2006**, *88*, 041914.
(20) David, W. I. F.; Jones, M.; Gregory, D.; Jewell, C.; Johnson, S.; Walton, A.; Edwards, P. P. *J. Am. Chem. Soc.* **2007**, *129*, 1594−1601.
(21) Chellappa, R. S.; Chandra, D.; Somayazulu, M.; Gramsch, S. A.; Hemley, R. J. *J. Phys. Chem. B* **2007**, *111*, 10785−10789.
(22) Huang, X.; Li, D.; Li, F.; Jin, X.; Jiang, S.; Li, W.; Yang, X.; Zhou, Q.; Zou, B.; Cui, Q.; Liu, B.; Cui, T. *J. Phys. Chem. C* **2012**, *116*, 9744−9749.
(23) The $P\bar{4}2_1m$ and $P4_2/ncm$ phases actually have different space groups in different pressure intervals. This is due to the tilting of amide anions along the *c*-axis and puckering of lithium layers. The sequence of space groups for the $P\bar{4}2_1m$ phase is $P2_12_1$ (0 to 10 GPa) → $P\bar{4}2_1m$ (10 to 50 GPa) → $P2_1$ (above 50 GPa), and for $P4_2/ncm$ phase, $P4_2/ncm$ (0 to 50 GPa) → $P2_1/c$ (above 50 GPa).
(24) Zhong, Y.; Zhou, H.; Hu., C.; Wang, D.; Rao, G. *J. Alloys Compd.* **2012**, *544*, 129−133.
(25) Arunan, E.; Desiraju, G. R.; Klein, R. A.; Sadlej, J.; Scheiner, S.; Alkorta, I.; Clary, D. C.; Crabtree, R. H.; Dannenberg, J. J.; Hobza, P.; Kjaergaard, H. G.; Legon, A. C.; Mennucci, B.; Nesbitt, D. *J. Pure Appl. Chem.* **2011**, *83*, 1619−1636; **2011**, *83*, 1637−1641.
(26) Boese, A. D.; Chandra, A.; Martin, J. M. L.; Marx, D. *J. Chem. Phys.* **2003**, *119*, 5965−5980.
(27) *Gmelins Handbuch der Anorganischen Chemie, Lithium, System Number 20*; Meyer, R.J., Ed.; Verlag Chemie: Weinhein, Germany, 1960; pp 270−273.
(28) Dove, M. T. *Am. Mineral.* **1997**, *82*, 213−244.
(29) Tang, W.; Sanville, E.; Henkelman, G. *J. Phys.: Condens. Matter* **2009**, *21*, 084204.
(30) Lazicki, A.; Yoo, C. W.; Evans, W. J.; Hu, M. Y.; Chow, P.; Pickett, W. E. *Phys. Rev. B* **2008**, *78*, 155133 and references therein..
(31) Lonie, D. C.; Zurek, E. *Comput. Phys. Commun.* **2011**, *182*, 372−387.
(32) Kresse, G.; Furthmüller, J. *Phys. Rev. B* **1996**, *54*, 11169−11186.
(33) Perdew, J. P.; Burke, K.; Ernzerhof, M. *Phys. Rev. Lett.* **1996**, *77*, 3865−3868.
(34) Blöchl, P. E. *Phys. Rev. B* **1994**, *50*, 17953−17979.
(35) Kresse, G.; Joubert, D. *Phys. Rev. B* **1999**, *59*, 1758−1775.
(36) Togo, A.; Oba, F.; Tanaka, I. *Phys. Rev. B* **2008**, *78*, 134106.
(37) Baroni, S.; Giannozzi, P.; Testa, A. *Phys. Rev. Lett.* **1987**, *58*, 1861−1864.

## ■ NOTE ADDED AFTER ASAP PUBLICATION

This Article was published ASAP on October 2, 2012, with an error in Figure 14b. The corrected version was reposted on October 11, 2012.